Atmospheric
Chemistry
and Physics
Discussions

Open Access

Using δ^{13}C-CH$_4$ and δD-CH$_4$ to constrain Arctic methane emissions

Nicola J. Warwick[1,2], Michelle L. Cain[1], Rebecca Fisher[3], James L. France[4], David Lowry[3], Sylvia E. Michel[5], Euan G. Nisbet[3], Bruce H. Vaughn[5], James W. C. White[5] and John A. Pyle[1,2]

[1]National Centre for Atmospheric Science, NCAS, UK.
[2]Department of Chemistry, University of Cambridge, Lensfield Road, Cambridge, CB2 1EW, UK.
[3]Department of Earth Sciences, Royal Holloway, University of London, Egham, TW20 0EX, UK.
[4]School of Environmental Sciences, University of East Anglia, Norwich, NR4 7TJ, UK.
[5]Institute of Arctic and Alpine Research (INSTAAR), University of Colorado, Boulder, CO 80309, USA.

Correspondence to: Nicola J. Warwick (Nicola.Warwick@atm.ch.cam.ac.uk)

Abstract. We present a global methane modelling study assessing the sensitivity of Arctic atmospheric CH$_4$ mole fractions, δ^{13}C-CH$_4$ and δD-CH$_4$ to uncertainties in Arctic methane sources. Model simulations include methane tracers coloured by source and isotopic composition and are compared with atmospheric data at four high northern latitude measurement sites. We find the model's ability to capture the magnitude and phase of observed seasonal cycles of CH$_4$ mixing ratios, δ^{13}C-CH$_4$ and δD-CH$_4$ in high northern latitudes is much improved using a later spring kick-off and autumn decline in high northern latitude wetland emissions than predicted by most process models. Results from our model simulations indicate that recent predictions of large methane emissions from thawing submarine permafrost in the East Siberian Arctic Shelf region could only be reconciled with global scale atmospheric observations by making large adjustments to high latitude emission inventories.

1 Introduction

Methane is an important greenhouse gas that has more than doubled in atmospheric concentration since pre-industrial times. Following a slow-down in the rate of growth in the late 1990s, the methane content of the atmosphere began increasing again in 2007. Although this increase has occurred globally, latitudinal differences in methane growth rates suggest multiple causes for the renewed growth. In 2007, the Arctic experienced a rapid methane increase, but in 2008 and 2009-10 growth was strongest in the tropics. This renewed global increase in atmospheric methane has been accompanied by a shift towards more ^{13}C-depleted values, suggesting that one explanation for the change could be an increase in ^{13}C-depleted wetland emissions (Nisbet et al., submitted). However, other factors such as changing emissions from ruminant animals (Schaefer et al., 2016) and the fossil fuel industry could also play a role.

The Arctic contains important methane sources that are currently poorly quantified and climate sensitive, with the potential for positive climate feedbacks. The largest and most uncertain of these are emissions from wetlands. While wetland methane fluxes can be obtained experimentally by chamber studies and eddy correlation techniques (e.g. Pelletier et al., 2007, O'Shea et al, 2014), the heterogeneous conditions in wetlands and seasonal and interannual variation in wetland area (Petrescu et al.,

Atmospheric
Chemistry
and Physics
Discussions

2010) can lead to large uncertainties, both spatially and temporally, when upscaling this data. As high latitude wetland emissions are generally considered to occur from May melt to October freeze-up (Bohn et al., 2015, Christensen et al., 2003), and due to difficulties conducting field campaigns during the winter and spring-melt seasons, to-date most experimental Arctic wetland flux data has been reported for the summer season. However, a recent Arctic wetland study

5   using year-round eddy flux data reported the presence of large methane emissions continuing well into winter, when subsurface soil temperatures remain close to 0°C (Zona et al., 2016). This study concluded that cold season (September-May) fluxes dominated the Arctic tundra methane budget.

Methane emissions from wetlands can also be estimated using process-based models. However, a recent model intercomparison study, WETCHIMP, showed wide disagreement in the magnitude of global and regional emissions among

10 large-scale models (Melton et al., 2013). The magnitude of methane emissions from high northern latitude wetlands (>50° N) varied from 21 to 54 Tg yr^{-1} (Melton et al., 2013), representing approximately 5 to 10 % of the total global methane emission budget. There was also significant variability between models in the seasonal distribution of these emissions. Figure 1 shows a comparison of seasonal cycles of high northern latitude wetland emissions from the WETCHIMP models, the wetland dataset described in Fung et al. (1991) and the model inversion study of Bousquet et al. (2011). There is significant spread in

15 how the emissions are distributed throughout the year, with the summertime peak in emissions occurring in June, July or August depending on the model considered. In a model intercomparison focusing on wetland emissions in West Siberia (WETCHIMP-WSL, Bohn et al., 2015), the largest disagreement in the temporal distribution of emissions occurs in springtime (May and June). During this period, the range in normalised model monthly emissions spans from a minimum of negative values (representing methane uptake) to a peak in the emission seasonal cycle. This large uncertainty associated

20 with the timing of, and processes controlling, seasonal variations in wetland methane emissions needs to be resolved before predictions can be made of how emissions might change in a changing climate.

Decomposing gas hydrates may also represent a small, but significant, climate sensitive methane source. Shallow methane hydrates in Arctic regions may be particularly vulnerable to destabilisation following increases in temperature as a result of climate change. Furthermore, thawing permafrost could release methane previously trapped below in shallow reservoirs,

25 including hydrates, to the atmosphere. Previous studies of the methane budget have either omitted a hydrate source or used a global value for Arctic hydrate emissions of 5 Tg yr^{-1}. However this value is no more than a placeholder suggested by Cicerone and Oremland (1988). More recently, Shakhova et al., (2010) and Shakhova et al. (2014) used ship-based observations to estimate methane emissions from thawing permafrost on the East Siberian Arctic Shelf (ESAS). They estimated a total ESAS methane source from diffusion, ebullition and storm-induced release from subsea permafrost and

30 hydrates of 17 Tg yr^{-1}; significantly more than the 5 Tg yr^{-1} suggested by Cicerone and Oremland (1988). However, a recent study by Berchet at al. (2016) using an atmospheric chemistry transport model, found that an ESAS source as high as 17 Tg yr^{-1} was inconsistent with atmospheric observations of methane mole fractions at northern high latitude measurement sites. In this study, ESAS emissions were estimated to be in the range 0.5 to 4.3 Tg yr^{-1}.

Atmospheric
Chemistry
and Physics
Discussions

Other recent studies identifying additional potential northern high latitude sources and sinks of methane include emissions from Arctic thermokarst lakes (11.86 Tg yr^{-1}, Tan and Zhuang, 2015), polymers in oceanic ice (~7 Tg yr^{-1}, Kort et al., 2012) and methane uptake by boreal vegetation (~-9 Tg yr^{-1}, Sundqvist et al., 2012). These studies have either used process-based models or extrapolated local observations to calculate Arctic fluxes that would all be highly significant on a regional scale.

5 However, uncertainties in these sources are high as many fluxes may be episodic as well as spatially scattered, and could therefore be missed by relatively infrequent field campaigns. In addition to natural sources, the Arctic contains methane emissions from some of the world's largest gas producing plants, situated in northern Russia (Reshetnikov et al., 2000).

The main atmospheric sink of methane is reaction with the hydroxyl radical, OH. Other lesser sinks include reaction with Cl in the boundary layer (e.g. Allan et al., 2007, Lawler et al., 2011, Banton et al., 2015) and uptake of methane by

10 methanotrophs in oxic soils. These sinks all vary seasonally due to seasonal changes in solar insolation and temperature etc., with peak destruction rates during the summer. Overall, knowledge of source and sink partitioning within the Arctic methane budget is poor, and a better understanding of emissions is required to determine the best emission reduction strategies and feedbacks in a future climate.

Along with atmospheric modelling, measurements of methane mole fractions provide important information on the

15 geographic and seasonal distribution of methane emissions. However, mole fraction measurements alone do not give us the ability to distinguish between emissions from different methane sources. This can be achieved in a broad sense using observations of stable isotope ratios in methane as different sources have distinct isotopic ratios. For example, methane emitted from wetlands is relatively more depleted in ^{13}C than that from fossil sources, which are in turn depleted relative to methane derived from biomass burning (Dlugokencky et al. 2011). To date, global atmospheric modelling studies have only

20 incorporated information on the ^{13}C/^{12}C ($\delta^{13}C_{CH4}$) composition of methane using geographically uniform source isotopic signatures. However, new information on the atmospheric distribution of the D/H composition (White et al, 2016) provides an additional potential discriminant between sources and source strengths. Here we present the first modelling study of modern methane to (a) include published large geographical variations in the isotopic signature of wetland emissions and (b) assess methane emission scenarios against atmospheric observations of δD_{CH4}.

25 Global model simulations are performed using the p-TOMCAT 3D chemistry transport model using offline chemistry (Warwick et al., 2006) and multiple methane tracers coloured by source and $\delta^{13}C$ and δD isotopic composition. We investigate the sensitivity of atmospheric distributions of CH_4, $\delta^{13}C_{CH4}$ and δD_{CH4} to changes in fluxes from climate-sensitive Arctic sources and analyse potential causes of differences between models and measurements in this region.

2 Measurements

30 Model results are compared to monthly mean weekly flask observations of CH_4 mixing ratios, $\delta^{13}C$-CH_4 and δD-CH_4 from NOAA-ESRL sampling sites at Alert (82°N, 63°W), Ny-Alesund (79°N, 12°E), Barrow (71°N, 157°W) and Cold Bay (55°N, 163°W) (Dlugokencky et al., 2013; White and Vaughn, 2015; White et al., 2016). These sites were selected for comparison as they are the four most northerly sites with simultaneous CH_4, $\delta^{13}C$-CH_4 and δD-CH_4 observation data.

Atmospheric
Chemistry
and Physics
Discussions

Monthly mean observations are averaged over the years 2005 to 2009 (the period for which there is δD-CH₄ data available). NOAA-ESRL was responsible for the collection of the sample and logistics, with cooperating agencies. Samples were then analysed for methane mixing ratios at NOAA-ESRL in Boulder, Colorado, with an analytical repeatability of 0.8 to 2.3 ppb. Stable isotopic compositions were determined at the Stable Isotope Laboratory at INSTAAR, part of the University of

5   Colorado, Boulder, with a precision of better than 0.1 ‰ for δ^{13}C-CH₄ (White et al., 2015; Miller et al., 2002) and 2‰ for δD-CH₄ (White et al., 2016).

3 Isotopic composition of methane

The isotopic composition of atmospheric methane is generally expressed in 'delta' notation, as the isotopic ratio in the sample compared to an international standard. The original standard for the ^{13}C/^{12}C ratio was Pee Dee Belemnite, a fossil

10   from the Pee Dee marine carbonate formation in South Carolina (Craig, 1957), which established the V-PDB scale. For the D/H ratio, the international standard is Vienna Standard Mean Ocean Water (VSMOW) (DeWitt et al., 1980). The delta values for the two main stable isotopologues of methane are given by

$$\delta^{13}C = 1000 \left(\frac{R_{13CH4}}{R_{PDB}} - 1 \right) \qquad (1)$$

$$\delta D = 1000 \left(\frac{R_{CH3D}}{R_{VSMOW}} - 1 \right) \qquad (2)$$

15   where R_x is the molar ratio of ^{13}C or D to the most abundant isotopologue (i.e. ^{12}C or H respectively). R_{PDB} is the ^{13}C/^{12}C ratio found in V-PDB and R_{VSMOW} is the D/H ratio found in V-SMOW. Global mean surface atmospheric observations of CH₄, δ^{13}C-CH₄ and δD-CH₄ are ~1800 ppb,~-47.3 ‰ and ~-86 ‰ respectively (Dlugokencky et al., 2013; White and Vaughn, 2015; White et al., 2016). Geographical and altitudinal variations in these compositions arise as a result of variations in the distributions of the isotopic composition of the parent organic matter, the method of production (pyrogenic,

20   thermogenic or biogenic) and differing rates of destruction between methane isotopologues. At large scales, the δD composition of methane is controlled by the δD of water present, while at smaller scales, the methods of production and destruction may play a more important role. Likewise the δ^{13}C composition of methane can be influenced by the type of parent organic matter (e.g. C3 or C4 vegetation), as well as the method of production. As different methane sources tend to have distinct isotopic ratios, observations of the isotopic composition of atmospheric methane can be used as additional

25   constraints on the methane budget (e.g. Rigby et al., 2013; Schaefer et al, 2016).

4 Model description

The global 3D chemical transport model, p-TOMCAT, has been used extensively for tropospheric studies and is described in more detail in Cook et al. (2007) and Warwick et al. (2013). For this study, the model was run at a horizontal resolution of ~2.8° x 2.8°, with 31 levels extending from the surface to 10 hPa. The horizontal and vertical transport of tracers was based

30   on 6-hourly meteorological fields, including winds and temperatures derived from the operational analyses of the European Centre for Medium Range Weather Forecasts (ECMWF) for 2009.

The version of p-TOMCAT used in this work has been modified to include parameterised chemistry where coloured-source methane tracers of $^{12}CH_4$ and $^{13}CH_4$, and a 'total' CH_3D are destroyed via reaction with OH, $O(^1D)$ and Cl. The OH distributions are prescribed hourly values taken from a full chemistry version of p-TOMCAT and compare well with other global OH distributions described in the literature, giving a global methane lifetime of 10.4 years with respect to OH (for

5 more details see Warwick et al., 2006). A comparison of modelled seasonal cycles of methyl chloroform and observational data from the NOAA-ESRL halocarbons in situ program at Barrow, Alaska, suggests that the seasonal cycle of the model prescribed OH concentrations is well represented in the Arctic region (see Fig. 2). Although there is a slight difference in the timing of the observed and modelled methyl chloroform minima, the modelled seasonal cycle falls well within the range of observations. The stratospheric destruction of methane by reaction with Cl and $O(^1D)$ is derived from prescribed 2D Cl and

10 $O(^1D)$ 5 day mean distributions taken from the Cambridge 2D model (Bekki and Pyle, 1994). Mixing ratios of Cl in the marine boundary layer are prescribed with latitudinal and seasonal variations according to Allan et al., (2007). Kinetic isotope effects (KIEs, defined as the ratio of rate constants for the reactions involving the reactant and an isotopically substituted reactant with a certain species) for the methane reaction rates are included in the model chemistry scheme and are listed in Table S1. Oxidation of methane by soils is treated as a negative emission following Fung et al., (1991).

15

Emissions used in the p-TOMCAT BASE scenario are described in Table S2. Prescribed surface methane fluxes are taken from EDGAR v4.1 (http://edgar.jrc.ec.europa.eu/overview.php?v=41) for 2005, Fung et al. (1991) and Van der Werf et al. (2006). The geographical distribution of wetland emissions above 50° N is shown in Fig. 3. Further details, including the source-specific isotopic signatures used in the model, are outlined in the Supplementary Online Material.

20 Initially, a 'total' methane tracer was spun-up in a 40-year single-tracer simulation until calculated year-to-year changes in local methane mole fractions were negligible. The coloured methane source tracers in each scenario were then initialised by scaling this spun-up total methane tracer globally, according to the global emission fraction and isotopic composition of the source. Results presented here are taken from the final year of further 40-year simulations using perpetual 2009 meteorology, after which year-to-year changes in the local mole fractions of the individual tracers were deemed to be negligible (<0.5 %),

25 along with the associated changes in $\delta^{13}C$-CH_4 and δD-CH_4.

5 Atmospheric distribution of methane mole fraction and isotopic composition

5.1 Global distribution

Figure 4 shows the modelled annual mean surface distributions of total CH_4, $\delta^{13}C$-CH_4 and δD-CH_4 for the BASE scenario. The results are broadly comparable to observational data, with higher mixing ratios and lighter (more negative) isotopic

30 fractionations occurring in the Northern Hemisphere (NH) than the Southern Hemisphere (SH). This gradient in isotopic fractionations arises as the rates of reaction of OH, Cl and $O(^1D)$ with $^{13}CH_4$ and CH_3D are all fractionally slower than with $^{12}CH_4$ (see Table S1). Therefore, both $\delta^{13}C$ and δD increase (become more enriched in the heavy isotope) with increased

exposure to atmospheric sinks. As the majority of methane emissions are located in the NH, and because these are predominantly depleted in heavy isotopes, there are strong latitudinal gradients in methane and its isotopic fractionations: higher concentrations and more negative δ^{13}C-CH$_4$ and δD-CH$_4$ values are found in the NH than the SH. Regional variations in δ^{13}C-CH$_4$ and δD-CH$_4$ also occur due to regional variations in methane source types with differing isotopic signatures (see Table S2).

The model captures the observed latitudinal gradients in CH$_4$, δ^{13}C-CH$_4$ and δD-CH$_4$, although the gradient in δD-CH$_4$ is underestimated in the model in northern mid-latitudes (see Fig. 5). These latitudinal gradients are likely to be strongly influenced by the representation of Arctic methane sources, particularly high latitude wetland emissions, which will give a strong isotopic atmospheric signal due to their very negative δ^{13}C-CH$_4$ and δD-CH$_4$ values. The sensitivity of the modelled latitudinal gradient to variations in particular Arctic methane sources is discussed in more detail in Sect. 6.

5.2 Arctic seasonal cycles

5.2.1 Comparison of the base simulation with observations

The observed seasonal cycle of CH$_4$ mole fractions in high northern latitudes is dominated by a sharp summer minimum in July, and a broader winter maximum from October to March (see Fig. 6). This seasonal cycle arises as a result of seasonal variations in the major methane sink, reaction with OH, seasonal variations in the surface sources of methane and seasonal changes in vertical mixing and horizontal transport. For example, the Arctic is influenced by long-range transport of airmasses containing high levels of anthropogenic methane from lower latitudes during winter and spring (e.g. Dlugokencky et al. 1995; Worthy et al. 2009). Model studies have had difficulty capturing seasonal cycles of methane in high northern latitudes (e.g. Houweling et al., 2000; Wang et al., 2004; Pickett-Heaps et al., 2011), in particular the timing of the summer minimum.

Observed seasonal cycles of δ^{13}C-CH$_4$ and δD-CH$_4$ show some level of anti-correlation with CH$_4$ mole fractions. If the seasonal cycle of CH$_4$ were due to reaction with OH alone, then the KIEs of the CH$_4$ + OH reaction would result in δ^{13}C-CH$_4$ and δD-CH$_4$ seasonal cycles 180° out of phase with the CH$_4$ seasonal cycle: the minimum in CH$_4$ mixing ratio corresponding to maxima in δ^{13}C-CH$_4$ and δD-CH$_4$. However, phase relationships between observed seasonal cycles in CH$_4$, δ^{13}C-CH$_4$ and δD-CH$_4$ are also influenced by seasonal variations in surface sources and lesser, alternate sinks leading to more complicated phase relationships.

The reaction of CH$_3$D with OH has a larger KIE than the reaction of ^{13}CH$_4$ with OH (see Table S1). Therefore seasonal variations in atmospheric δD-CH$_4$ will tend to be more dominated by seasonal changes in the OH sink than δ^{13}C-CH$_4$, with atmospheric δ^{13}C-CH$_4$ being relatively more influenced by sources. Figure 6 shows that the observed seasonal cycle of δD-CH$_4$ is approximately anti-correlated with CH$_4$, as would be expected for a seasonal cycle controlled by seasonal variations in OH. However, this is not true for δ^{13}C-CH$_4$. There is an offset between the CH$_4$ and δ^{13}C-CH$_4$ seasonal cycles, with a period in late spring where CH$_4$ decreases and there is either no change or a slight decrease in δ^{13}C-CH$_4$. In addition, a

Atmospheric
Chemistry
and Physics
Discussions

simultaneous increase in both observed CH_4 and $\delta^{13}C$-CH_4 from October through to the end of the year demonstrates that factors other than seasonal variations in OH play a role in determining the seasonal cycle of $\delta^{13}C$-CH_4.

Figure 6 also shows a comparison of modelled seasonal cycles of CH_4, $\delta^{13}C$-CH_4 and δD-CH_4 from the BASE scenario with observational data from four high northern latitude sites. Although the model captures the phase and magnitude of observed seasonal cycles in lower northern latitudes (e.g. Cold Bay), clear differences in the magnitude and/or phase are evident in higher latitudes (Alert, Ny-Alesund, Barrow). The model is unable to capture the magnitude and timing of the Arctic summer minimum in CH_4 mixing ratios, while the modelled summer decrease in $\delta^{13}C$-CH_4 and δD-CH_4 occurs earlier than observed. In addition, the model underestimates the amplitude of the observed Arctic seasonal cycle in δD-CH_4. These discrepancies point to errors in the representation of Arctic methane sources and/or the isotopic signature data used within the model. In Sect. 6, we investigate the sensitivity of modelled seasonal cycles to uncertainties in the δD KIE for the CH_4 + OH reaction, as well as adjustments in the phase and magnitude of certain Arctic sources.

6 Model sensitivities to Arctic source magnitudes and δD isotopic signatures and fractionations

6.1 Model sensitivity to $KIE^{H/D}$ and the wetland δD signature

Although the model is able to capture the phase and magnitude of observed seasonal cycles of methyl chloroform in the Arctic, suggesting that the OH seasonal cycle is well represented (Fig. 2), the model underestimates the amplitude of Arctic seasonal cycles of both CH_4 and δD-CH_4 (Fig. 6). In two further separate model simulations, we investigated the sensitivity of Arctic modelled seasonal cycles in δD-CH_4 to (a) uncertainties in the KIE of the CH_3D + OH reaction and (b) uncertainties in the δD signature of methane emissions from high northern latitude wetlands.

Literature KIE values for $k^{CH4+OH}/k^{CH3D+OH}$ range from 1.16 to 1.3, clustering at the higher end of range (DeMore et al., 1993; Gierczak et al., 1997; Bergamaschi et al., 2000; Saueressig et al., 2001; Tyler et al., 2007). In a separate model simulation run parallel to the BASE simulation, we find that altering the $KIE^{CH3D+OH}$ reaction within the literature range has an important impact on modelled global mean δD-CH_4 values. However, we found the impact of varying $KIE^{CH3D+OH}$ on the magnitude of the modelled δD-CH_4 seasonal cycle to be negligible, offering no improvement over the BASE scenario when comparing with observations.

While there is now an increasing amount of data on $^{13}C/^{12}C$ source ratios, D/H ratios for methane sources have been less comprehensively studied and are therefore subject to larger uncertainties. Literature estimates of the δD-CH_4 isotopic signature from high northern latitude wetlands range from approximately -300 ‰ to -450 ‰ (e.g. Kulmann et al., 1998; Quay et al, 1999; Nakagawa et al., 2002; Umezawa et al., 2012). However, bulk regional δD values for western Siberian emissions estimated by Yamada et al. (2005) (-482 ‰ to -420 ‰, including the major wetland and fossil fuel sources) suggest a more negative δD signature for wetlands than determined by other studies. Here we found that increasing the isotopic signature of >50° N wetland emissions from -360 ‰ to -500 ‰ much improved the ability of the model to capture the magnitude of the observed seasonal cycle and latitudinal gradient of δD-CH_4 (not shown). However, using such a

negative δD signature for high northern latitude wetland emissions would obviously shift the model global mean δD-CH$_4$ to more negative values, and would therefore have to be balanced by further altering the source/sink scenario. In addition, while altering the δD wetland source signature improves the representation of the modelled δD-CH$_4$ seasonal cycle, it does not impact the differences between the modelled and observed CH$_4$ seasonal cycles.

6.2 Model sensitivity to the wetland source

6.2.1 Varying the source magnitude

Emissions from high northern latitude wetlands (>50° N) are assigned a highly ^{13}C-depleted and D-depleted isotopic signature (~-70‰ and ~-360‰ respectively) in the model, as well as a strong seasonal cycle, peaking during the NH summer. Therefore reducing methane emissions from high latitude wetlands in early summer could potentially improve the comparison between observed and modelled seasonal cycles of CH$_4$, δ^{13}C-CH$_4$ and δD-CH$_4$. Figure 7 shows the influence of varying the magnitude of the wetland source above 50° N on the phase and magnitude of modelled high latitude NH CH$_4$ and δ^{13}C-CH$_4$ seasonal cycles. No results for δD-CH$_4$ are shown as CH$_3$D was not coloured by source in the model due to computer integration time limitations.

When the coloured high northern latitude (>50° N) wetland methane tracer (with emissions of 30 Tg yr^{-1}) is excluded from the model simulation (NO_WETLD scenario), the summer minimum in CH$_4$ mole fraction occurs later in the year (August/September) than in the BASE scenario and the seasonal variation in δ^{13}C-CH$_4$ is substantially reduced (Fig. 7). When high northern latitude wetland emissions are increased by 50 % (i.e. the annual source strength is increased to 45 Tg yr^{-1}, WETLD_X2 scenario), the summer minimum occurs earlier in the year (May/June) and seasonal variations in both CH$_4$ and δ^{13}C-CH$_4$ increase relative to the BASE scenario (Fig. 7). Neither wetland scenario provides any improvement in the model's ability to capture observed seasonal cycles: the comparison with observations is much worse when high northern latitude wetland emissions are removed, and there are only small changes to model results when high northern latitude wetland emissions are increased by 50 %.

Figure 8 shows the influence of varying the strength of wetland emissions above 50° N on the modelled latitudinal gradients of CH$_4$ and δ^{13}C-CH$_4$. Removing this source completely dramatically reduces the ability of the model to capture observed latitudinal gradients: the modelled interpolar gradient in δ^{13}C-CH$_4$ is reduced by ~75 % from ~0.4 ‰ to 0.1 ‰, and the gradient in CH$_4$ mixing ratios by ~22 % in the NO_WETLD scenario relative to the BASE scenario. Increasing high northern latitude wetland emissions by 50 % increases the interpolar difference in both CH$_4$ and δ^{13}C-CH$_4$ in the WETLD_X2 scenario relative to the BASE scenario. In this case, the gradient in CH$_4$ mole fractions is then slightly overestimated.

Atmospheric
Chemistry
and Physics
Discussions

6.2.2 Varying the phase of the seasonal cycle

To investigate the impact of the prescribed phase of the seasonal cycle of high latitude wetland methane emissions on modelled atmospheric distributions of CH_4, $\delta^{13}C$-CH_4 and δD-CH_4, a further model scenario is run (DEL_WET) in which the seasonal cycle of this source is delayed by one month, resulting in a later spring kick-off in emissions and a decline in

5 emissions that occurs later in autumn than in the BASE scenario. While this has a negligible influence on the modelled latitudinal gradient (not shown), shifting the high latitude wetland emission seasonal cycle forward in the year by one month (so the summer emission season starts and finishes one month later in the year) has a notable impact on modelled seasonal variations in atmospheric methane and its isotopic composition (see Fig. 9). In this case, the model is better able to capture observed seasonal cycles in CH_4, $\delta^{13}C$-CH_4 and δD-CH_4.

10 These results do not support the existence of a large spring burst in wetland emissions as has been reported in other studies (e.g. Christensen et al., 2004; Song et al., 2012). To capture the correct timing of the CH_4 minima and $\delta^{13}C$-CH_4 and δD-CH_4 maxima, the model requires that there be no large contribution from wetland emissions until June, with peak emissions occurring between July and September. Equally, to capture the correct timing of the summer/autumn increase in CH_4 mixing ratios and decrease in $\delta^{13}C$-CH_4, the model requires strong contributions from an isotopically light source continuing through

15 to November. This could be from autumnal wetland emissions, as represented here. A large late-autumnal high northern latitude wetland source is supported by the recent work of Zona et al., (2016), who observed strong methane fluxes at an Arctic wetland site continuing well after the near-surface soil layer starts to freeze in late August or early September. Alternatively, it is possible that the comparison between modelled and observed $\delta^{13}C$-CH_4 (though not CH_4 mixing ratios) could be improved by prescribing a seasonal variation to the signature of high northern latitude wetland emissions as

20 observed by Sriskantharajah et al. (2012).

6.3 Model sensitivity to the hydrate / thawing permafrost source

Methane emissions from ocean bottom decomposing hydrates and thawing permafrost in the Arctic are not well known due to uncertainties in the amount of carbon in permafrost, the sizes and locations of the methane hydrate deposits, the rate of heat transfer through the ocean and sediments, and the fate of methane once it has been released into sea water (O'Connor et

25 al. 2010). A recent study by Shakhova et al. (2014) estimated methane emissions of 17 Tg yr^{-1} from the ESAS based on extrapolation of field observations in the Southern Laptev Sea. An emission of this magnitude represents a substantial reassessment of the high northern latitude methane budget, being equivalent to ~25 % of total estimated methane emissions above 50° N. A subsequent study by Berchet et al. (2016) reported that an ESAS flux of this magnitude was inconsistent with atmospheric observations, and used a statistical analysis of observations and model simulations to estimate an ESAS

30 source of 0.5 to 4.3 Tg yr^{-1}.

To assess the sensitivity of the model to uncertainties in this high latitude methane source, we compare three scenarios in which methane emissions from the East Siberian Arctic Shelf region are assigned magnitudes of 0, 5 and 17 Tg yr^{-1}

(NO_HYD, BASE and INC_HYD scenarios respectively). These emissions are set to be constant throughout the year as about 10 % of the ESAS remains open water in winter due to the formation of polynyas, implying that it could be a source of CH_4 to the atmosphere year-round (Shakhova et al. 2015), and due to the lack of any further data on seasonality. However, it is possible that summer ESAS fluxes, when the region is ice-free, could be larger than winter fluxes. The influence of these changes in emissions on the modelled latitudinal gradient is shown in Fig. 10. Although the magnitude of change in emission is small in comparison to the global budget (<~3 %), varying the strength of the ESAS source has a notable impact on modelled interpolar differences as the source is highly localised at high latitudes. In the scenario in which East Siberian Arctic Shelf emissions have been removed (NO_HYD), northern high latitude gradients in modelled CH_4 and $\delta^{13}C\text{-}CH_4$ are underestimated relative to observations. This demonstrates that the model does require a small, very high latitude, isotopically light source to capture observed latitudinal gradients, given the prescribed geographical distributions of emissions from other high latitude sources used in the BASE scenario. However, when ESAS hydrate emissions are increased to 17 Tg yr^{-1} (INC_HYD), the model predicts a larger latitudinal gradient in CH_4 between mid and high northern latitudes than seen in the observations. Therefore our model simulations do not support the existence of an East Siberian Arctic Shelf methane source of this magnitude, given the representations of other methane sources outlined in Table S2.

It is, however, possible that an East Siberian Arctic Shelf source of 17 Tg yr^{-1} could be accommodated in our model set-up if adjustments were made to the representation of other high northern latitude sources within the model. At 30 Tg yr^{-1}, wetlands represent the largest single methane source in high latitude regions (Table S2), and therefore have the largest potential for flux adjustment. We consider an alternative scenario (WET_HYD) including emissions of 17 Tg yr^{-1} from the East Siberian Arctic Shelf, but only 18 Tg yr^{-1} from high northern latitude wetlands (i.e. high northern latitude wetland emissions are geographically uniformly reduced by 12 Tg yr^{-1} and total NH emissions remain the same as in the BASE scenario). In this case, the modelled latitudinal gradient of CH_4 is in better agreement with the observations than INC_HYD. However in WET_HYD, the latitudinal gradient in $\delta^{13}C\text{-}CH_4$ is reduced relative to both observations and the BASE scenario in northern mid-latitudes (Fig. 10). This occurs as the isotopic signature of hydrate/permafrost emissions assigned in the model is larger than that of high latitude wetland emissions (~-55 ‰ compared to ~-70 ‰, see discussion below). In addition to the impact on the latitudinal gradient, the agreement of the model with observed seasonal cycles of CH_4, $\delta^{13}C\text{-}CH_4$ and $\delta D\text{-}CH_4$ is also reduced in high northern latitudes following the 12 Tg yr^{-1} reduction in high northern latitude wetland emissions (not shown). However, this is based on the use of constant ESAS emissions and inclusion of a seasonal cycle may influence our results.

These results are, at least partly, based on the assumption that the isotopic signatures assigned to high northern latitude wetlands and ocean floor hydrates/thawing permafrost are correct, and specifically that the $\delta^{13}C$ signature for wetland emissions is more negative than that for hydrates/permafrost. $\delta^{13}C$ signatures for Arctic wetland emissions have been determined in a number of studies and there is strong agreement that these emissions are highly depleted in ^{13}C, with values <-65 ‰ (Fisher et al., 2011, Sriskantharajah et al., 2012, O'Shea et al., 2015). Our value of -70 ‰ is based on recent data from the NERC MAMM (Methane in the Arctic: Measurements, process studies and Modelling) campaign (O'Shea et al.,

2015). δ^{13}C signatures from ocean floor hydrates and permafrost are less well known and as far as we are aware, have not been published for the Laptev Sea region. Measurements taken from decomposing CH_4 hydrate in sediment cores in the Norwegian Arctic show a wide δ^{13}C isotopic range, from ~-72 ‰ to ~-46 ‰ (Milkov, 2005; Vaular et al., 2010, Fisher et al., 2011). However, methane released from the sea floor will be oxidised in the water column and enriched in ^{13}C before

5 reaching the atmosphere as methanotrophs in ocean water would preferentially consume the lighter isotope. Therefore the isotopic signature of emission to the atmosphere will be more enriched in ^{13}C (less negative δ^{13}C) than the δ^{13}C values from sediment cores (Graves et al., 2015). A substantially lighter isotopic signature for ESAS methane emissions, as would be required to capture atmospheric δ^{13}C-CH_4 observations, is possible, however it would require both (a) a very light initial isotopic composition on release at the sea floor and (b) very limited oxidation in the water column before release to the

10 atmosphere. These factors could be achieved with a shallow sea floor (as is present for the ESAS) and the formation of large methane bubbles.

To assess how a more negative δ^{13}C signature for ESAS hydrate/permafrost emissions would influence our model results, we construct a further WET_HYD scenario for δ^{13}C-CH_4 in which the ESAS source of 17 Tgyr^{-1} is assigned a δ^{13}C signature of -70 ‰. In this case, the model simulates a much larger gradient in δ^{13}C-CH_4 in high northern latitudes than is seen in the

15 observations (Fig. 10). Therefore, whether a ESAS source of 17 Tgyr^{-1} can be accommodated in our global model along with a reduction in high northern latitude wetland emissions is highly dependent on the δ^{13}C signature used for the respective sources. Our model simulations indicate that if the ESAS source has a very negative δ^{13}C signature (-70 ‰ or more negative), then such a large, localised, high latitude source would strongly influence global scale hemispheric gradients.

The sum of all other (mostly anthropogenic) sources >50° N is ~37 Tg yr^{-1} (see Table S2). The isotopic compositions of

20 these sources are all either similar to, or heavier than the isotopic signature assigned to the East Siberian Arctic Shelf source in our BASE scenario (-55 ‰). Therefore is it possible that East Siberian Arctic Shelf emissions of 17 Tg yr^{-1} with a δ^{13}C value of -55 ‰ could be accommodated in model simulations of CH_4 and δ^{13}C-CH_4, provided substantial reductions in high latitude anthropogenic emissions of methane (for example ~50 % across all sources) are also included in the simulations. In this case the agreement between the modelled and observed interpolar difference in CH_4 and δ^{13}C-CH_4, and the high northern

25 latitude seasonal cycles of CH_4, δ^{13}C-CH_4 and δD-CH_4 could potentially be maintained. However, these scenarios could not be tested here as anthropogenic emissions were not coloured by latitude within the model. Such large flux adjustments to high latitude anthropogenic sources would indicate the presence of major systematic errors in the current inventories of high latitude emissions.

In summary, to accommodate an ESAS source of ~17 Tg yr^{-1} in our model simulations requires a substantial revision of our

30 emission scenario in high northern latitudes. We require either:

(a) A reduction in wetland emissions north of 50° N of ~40 % (i.e. totalling ~18 Tg yr^{-1}, a number just below the minimum of a range of process model studies), and ESAS emissions to have a seasonality and highly depleted isotopic signature similar to high northern latitude wetlands (i.e. peaking during the summer ice-free period).

Atmospheric
Chemistry
and Physics
Discussions

(b) A reassessment of anthropogenic methane emission inventories in which total emissions above 50° N are reduced by approximately 50 %, and ESAS emissions are emitted approximately constantly through the year with an isotopic signature close to anthropogenic emissions (~50 ‰)

(c) A combination of the above

5   (d) The inclusion of an additional, as yet unrepresented, high latitude sink, such as the boreal plant sink outlined in Sundqvist et al. (2012).

7 Implications for Arctic sources

Model studies disagree over the magnitude and seasonal distribution of high northern latitude wetland methane emissions (Melton et al., 2013; Bohn et al. 2015). This disagreement needs to be resolved in order to better predict future wetland

10   emissions in a warming climate. In this study, we find that high northern latitude wetland emissions have an important influence on both the magnitude and phase of high northern latitude seasonal cycles of CH_4 mixing ratios, $\delta^{13}C$-CH_4 and δD-CH_4. To date, measurements of δD source signatures are more limited than for $\delta^{13}C$, and uncertainties in source δD and $KIE^{H/D}$ values limit the conclusions that can be drawn from measurement-model comparisons of atmospheric data. However, with improved data, our model study shows that atmospheric observations of δD-CH_4, as well as $\delta^{13}C$-CH_4 could provide an

15   important constraint on current emissions from Arctic wetlands and inter-annual trends in this climate-sensitive source.

In our model simulations, the model's ability to capture the magnitude and observed seasonal cycles of CH_4 mixing ratios, $\delta^{13}C$-CH_4 and δD-CH_4 in high northern latitudes is much improved if the seasonal cycle of the Fung et al. (1991) wetland emissions is delayed by one month (i.e. the wetland emission season starts and finishes one month later than in the prescribed dataset). How this is interpreted will depend on the time-resolution of the emission dataset (one month for Fung et

20   al., (1991)), and the temporal method of implementation in the model. In p-TOMCAT, emissions are linearly interpolated in time from the centre-point of the month. However, with improved temporal resolution of emissions, perhaps a better agreement could be obtained without the need to delay the seasonal cycle.

Figure 1 shows a comparison of seasonal cycles in high northern latitude wetland emissions from Fung et al. (1991) compared to emission data from wetland process models obtained as part of the recent WETCHIMP model comparison

25   (Melton et al. 2013) and the methane model inversion study of Bousquet et al. (2011). The resulting emission distribution from delaying the Fung et al. (1991) seasonal cycle by one month generally falls within the range of model uncertainties, with the phase and shape of the seasonal cycle (though not emission magnitude) most closely matching that of the LPJ-Bern model. However, the delayed start to the emissions results in notably smaller emissions in May than predicted by the other studies. Lower May-time emissions than predicted could be a result of continued snow cover at high latitudes or high water

30   levels during the melt season limiting the amount of CH_4 released to the atmosphere due to oxidation in the water column. In addition, spring increases in CH_4 uptake by oxic forest soils and/or the canopy could contribute towards lower net emissions from high latitudes in May (Sundqvist et al. 2012).

Atmospheric
Chemistry
and Physics
Discussions

p-TOMCAT also requires a larger autumnal isotopically 'light' methane source than predicted by most wetland models to capture observed seasonal cycles of CH_4, $\delta^{13}C$-CH_4 and δD-CH_4. This result is consistent with a recent study by Zona et al., (2016) measuring year-round wetland fluxes at an Arctic wetland site. They found large methane fluxes continuing throughout the 'zero curtain' period, where subsurface soil temperatures remain active at ~0°C before freezing around

5   December time, partly due to the insulating effects of snow cover. Other possible contributions towards an additional, isotopically light, autumnal methane source include processes releasing methane during tundra freezing (Mastepanov et al. 2008).

Using current literature estimates for northern high latitude methane emissions, our study suggests an ESAS methane source in the lower half of published estimated ranges (0.5 to 17 Tg yr^{-1}). This is in agreement with the study by Berchet et al.

10   (2016), which used synoptic data from long-term methane measurement sites to constrain ESAS emissions from 0.5 to 4.3 Tg yr^{-1}. We find that substantial adjustments in estimates of high latitude methane source flux magnitudes or isotopic source signatures are required in order to reconcile East Siberian Arctic Shelf emissions as large as 17 Tg yr^{-1} with global scale atmospheric observations of CH_4 and $\delta^{13}C$-CH_4. Depending on currently lacking information on the seasonality and isotopic signature of an ESAS source, these include reducing high northern latitude wetland emissions by ~40 % (to a value just

15   below the minimum of a range of values predicted by process models), reducing high northern latitude emissions from anthropogenic emission inventories by ~50 % or a combination of the two. Alternatively, a missing seasonal sink, such as the destruction of methane by boreal vegetation suggested by Sundqvist et al. (2012) could help reconcile large emissions from the ESAS with global scale atmospheric observations. Further information on the isotopic signature and seasonality of an ESAS source would be of benefit in distinguishing between possible scenarios.

20   **Acknowledgements**

25   **References**

Allan, W., Struthers, H., and Lowe, D. C.: Methane carbon isotope effects caused by atomic chlorine in the marine boundary layer: Global model results compared with Southern Hemisphere measurements, J. Geophys. Res., 112, D04306, doi:10.1029/2006JD007369, 2007.

Bekki, S., and Pyle, J. A., A two-dimensional modeling study of the volcanic eruption of Mount Pinatubo, J. Geophys. Res.,
30   99(D9), 18861–18869, doi:10.1029/94JD00667, 1994.

Atmospheric
Chemistry
and Physics
Discussions

Bergamaschi, P., Bräunlich, M., Marik, T., and Brenninkmeijer, C. A. M.: Measurements of the carbon and hydrogen isotopes of atmospheric methane at Izaña, Tenerife: Seasonal cycles and synoptic-scale variations, J. Geophys. Res., 105(D11), 14531–14546, doi:10.1029/1999JD901176, 2000.

Berchet, A., Bousquet, P., Pison, I., Locatelli, R., Chevallier, F., Paris, J.-D., Dlugokencky, E. J., Laurila, T., Hatakka, J., Viisanen, Y., Worthy, D. E. J., Nisbet, E. G., Fisher, R. E., France, J. L., Lowry, D., Ivakhov, V., and Hermansen, O.: Atmospheric constraints on the methane emissions from the East Siberian Shelf, Atmos. Chem. Phys., 16, 4147-4157, doi:10.5194/acp-16-4147-2016, 2016.

Bohn, T. J., Melton, J. R., Ito, A., Kleinen, T., Spahni, R., Stocker, B. D., Zhang, B., Zhu, X., Schroeder, R., Glagolev, M. V., Maksyutov, S., Brovkin, V., Chen, G., Denisov, S. N., Eliseev, A. V., Gallego-Sala, A., McDonald, K. C., Rawlins, M.A., Riley, W. J., Subin, Z. M., Tian, H., Zhuang, Q., Kaplan, J. O.: WETCHIMP-WSL: intercomparison of wetland methane emissions models over West Siberia, Biogeosciences, 12, 3321—3349, doi:10.5194/bg-12-3321-2015, 2015.

Born, M., Dörr, H. and Levin, I: Methane consumption in aerated soils of the temperate zone. Tellus B, 42, 2–8, doi: 10.1034/j.1600-0889.1990.00002.x, 1990.

Bousquet, P., Ringeval, B., Pison, I., Dlugokencky, E. J., Brunke, E.-G., Carouge, C., Chevallier, F., Fortems-Cheiney, A., Frankenberg, C., Hauglustaine, D. A., Krummel, P. B., Langenfelds, R., L. , Ramonet, M., Schmidt, M., Steele, L. P., Szopa, S., Yver, C., Viovy, N. and Ciais, P.: Source attribution of the changes in atmospheric methane for 2006–2008, Atmos. Chem. Phys., 11, 3689–3700, doi:10.5194/acp-11-3689-2011, 2011.

Christensen, T. R., Ekberg, A., Ström, L., Mastepanov, M., Panikov, N., Öquist, M., Svensson, B. H., Nykänen, H., Martikainen, P. J., and Oskarsson, H., Factors controlling large scale variations in methane emissions from wetlands, Geophys. Res. Lett., 30, 1414, doi:10.1029/2002GL016848, 2003.

Christensen, T. R., Johansson, T., Akerman, H. J. and Mastepanov, M.: Thawing sub-arctic permafrost: effects on vegetation and methane emissions, Geophys. Res. Lett., 31, L04501, 2004.

Cicerone, R. J., and Oremland, R. S., Biogeochemical aspects of atmospheric methane, Global Biogeochemical Cycles, 2, 299-327, doi:10.1029/GB002i004p00299, 1988.

Cook, P. A., Savage, N. H., Turquety, S., Carver, G. D., O'Connor, F. M., Heckel, A., Stewart, D., Whalley, L. K., Parker, A. E., Schlager, H., Singh, H. B., Avery, M. A., Sachse, G. W., Brune, W., Richter, A., Burrows, J. P., Purvis, R., Lewis, A. C., Reeves, C. E., Monks, P. S., Levine, J.G. and Pyle, J. A.: Forest fire plumes over the North Atlantic: p-TOMCAT model simulations with aircraft and satellite measurements from the ITOP/ICARTT campaign, J. Geophys. Res., 112, D10S43, doi:10.1029/2006JD007563, 2007.

Craig, H., Isotope standards for carbon and oxygen and correction factors for mass-spectrometric analysis of carbon dioxide, Geochirn. Cosrnochirn. Acta, 12, 133-149, 1957.

DeMore, W. B., Rate constant ratio for the reaction of OH with CH3D and CH4, J. Phys. Chem., 97, 8564–8566, 1993.

DeWit, J.C., Van der Straaten, C.M. and Mook, W.G.: Determination of the absolute hydrogen isotopic ratio of V-SMOW and SLAP, Geostand. Newsl., 4, (1), 33-36, 1980.

Dlugokencky, E. J., Steele, L. P., Lang, P. M., and Masarie, K. A.: Atmospheric methane at Mauna Loa and Barrow observatories: Presentation and analysis of in situ measurements, J. Geophys. Res., 100(D11), 23103–23113, doi:10.1029/95JD02460, 1995.

Dlugokencky, E. J., Nisbet, E. G., Fisher, R., and Lowry, D.: Global atmospheric methane: budget, changes and dangers, Phil. Trans. R. Soc. A, 369, 2058-2072; doi: 10.1098/rsta.2010.0341, 2011.

Dlugokencky, E.J., Lang, P. M., Crotwell, A. M., Masarie, K. A. and Crotwell, M. J.: Atmospheric Methane Dry Air Mole Fractions from the NOAA ESRL Carbon Cycle Cooperative Global Air Sampling Network, 1983-2012, Version: 2013-08-28, Path: ftp://aftp.cmdl.noaa.gov/data/trace_gases/ch4/flask/surface/, 2013.

Fisher, R. E., Sriskantharajah, S., Lowry, D. , Lanoisellé, M., Fowler, C. M. R., James, R. H., Hermansen, O., Lund Myhre, C., Stohl, A., Greinert, J., Nisbet-Jones, P. B. R., Mienert, J., Nisbet, E. G.: Arctic methane sources: Isotopic evidence for atmospheric inputs, Geophys. Res. Lett., 38, L21803, doi:10.1029/2011GL049319, 2011.

Fung, I., John, J., Lerner, J., Matthews, E., Prather, M., Steele, L. P., and Fraser, P. J.: Three-dimensional model synthesis of the global methane cycle, J. Geophys. Res., 96, 13033-13065, doi:10.1029/91JD01247, 1991.

Gierczak, T., Talukdar, R. K., Herndon, S. C., Vaghjiani, G. L., and Ravishankara, A. R.: Rate Coefficients for the Reactions of Hydroxyl Radicals with Methane and Deuterated Methanes, The Journal of Physical Chemistry, 101 (17), 3125-3134, doi: 10.1021/jp963892r, 1997.

Graves, C. A., Steinle, L., Rehder, G., Niemann, H., Connelly, D. P., Lowry, D., Fisher, R. E., Stott, A. W., Sahling, H., and James, R. H., Fluxes and fate of dissolved methane released at the seafloor at the landward limit of the gas hydrate stability zone offshore western Svalbard, J. Geophys. Res. Oceans, 120, 6185–6201, doi:10.1002/2015JC011084, 2015.

Houweling, S., Dentener, F., Lelieveld, J., Walter, B., and Dlugokencky, E.: The modeling of tropospheric methane: How well can point measurements be reproduced by a global model?, J. Geophys. Res., 105, 8981-9002, doi:10.1029/1999JD901149, 2000.

Kort, E. A., Wofsy, S. C., Daube, B. C., Diao, M., Elkins, J. W., Gao, R. S., Hintsa, E. J., Hurst, D. F., Jimenez, R., Moore, F. L., Spackman, J. R. and Zondlo, M. A.: Atmospheric observations of Arctic Ocean methane emissions up to 82° north, Nature Geoscience 5, 318–32, doi:10.1038/ngeo1452, 2012.

Kuhlmann, A. J., Worthy, D. E. J., Trivett, N. B. A. and Levin, I.: Methane emissions from a wetland region within the Hudson Bay Lowland: An atmospheric approach, J. Geophys. Res., 103(D13), 16009–16016, doi:10.1029/98JD01024, 1998.

Lawler, M. J., Sander, R., Carpenter, L. J., Lee, J. D., von Glasow, R., Sommariva, R., and Saltzman, E. S.: HOCl and Cl2 observations in marine air, Atmos. Chem. Phys., 11, 7617-7628, doi:10.5194/acp-11-7617-2011, 2011.

Mastepanov, M., Sigsgaard, C., Dlugokencky, E. G., Houweling, S., Ström, L., Tamstorf, M. P. and Christensen, T. R.: Large tundra methane burst during onset of freezing, Nature, 456, 628-630, doi:10.1038/nature07464, 2008.

Melton, J. R., Wania, R., Hodson, E. L., Poulter, B., Ringeval, B., Spahni, R., Bohn, T., Avis, C. A., Beerling, D. J., Chen, G., Eliseev, A. V., Denisov, S. N., Hopcroft, P. O., Lettenmaier, D. P., Riley, W. J., Singarayer, J. S., Subin, Z. M., Tian, H., Zurcher, S., Brovkin, V., van Bodegom, P. M., Kleinen, T., Yu, Z. C., and Kaplan, J. O.: Present state of global wetland

extent and wetland methane modelling: conclusions from a model inter-comparison project (WETCHIMP), Biogeosciences, 10, 753–788, doi:10.5194/bg-10-753-2013, 2013.

Milkov, A. V., Molecular and stable isotope compositions of natural gas hydrates: A revised global dataset and basic interpretations in the context of geological settings, Org. Geochem., 36(5), 681-702, doi:10.1016/j.orggeochem.2005.01.010,

5   2005.

Miller, J. B., K. A. Mack, R. Dissly, J. W. C. White, E. J. Dlugokencky, and P. P. Tans, Development of analytical methods and measurements of 13C/12C in atmospheric CH4 from the NOAA Climate Monitoring and Diagnostics Laboratory Global Air Sampling Network, J. Geophys. Res., 107(D13), doi:10.1029/2001JD000630, 2002.

Nakagawa, F., Yoshida, N., Nojiri, Y., Makarov, V. N.: Production of methane from alasses in eastern Siberia: Implications

10   from its 14C and stable isotopic compositions, Global Biogeochem. Cycles, 16(3), doi:10.1029/2000GB001384, 2002.

Nisbet, E.G., Dlugokencky, E. J., Manning, M. R., Lowry, D., Fisher, R. E., France, J. L., Michel, S. E., Miller, J. B., White, J. W. C., Vaughn, B., Bousquet, P., Pyle, J. A., Warwick, N. J., Cain, M., Brownlow, R., Zazzeri, G., Lanoisellé, M., Manning, A. C., Gloor, E., Worthy, D. E. J., Brunke, E.-G., Labuschagne, C., Wolff, E. W. and Ganesan, A. L., Rising atmospheric methane: 2007-2014 growth and isotopic shift, submitted to Global. Biogeochem. Cyc..

15   O'Shea, S. J., Allen, G., Gallagher, M. W., Bower, K., Illingworth, S. M., Muller, J. B. A., Jones, B. T., Percival, C. J., Bauguitte, S. J-B., Cain, M., Warwick, N., Quiquet, A., Skiba, U., Drewer, J., Dinsmore, K., Nisbet, E. G., Lowry, D., Fisher, R. E., France, J. L., Aurela, M., Lohila, A., Hayman, G., George, C. , Clark, D. B., Manning, A. J., Friend, A. D. and Pyle, J., Methane and carbon dioxide fluxes and their regional scalability   for the European Arctic wetlands during the MAMM project in summer 2012, Atmos. Chem. Phys., 14, 13159-13174, doi: 10.5194/acp-14-13159-2014, 2014.

20   Pelletier, L., T. R. Moore, N. T. Roulet, M. Garneau, and V. Beaulieu-Audy, Methane fluxes from three peatlands in the La Grande Riviere watershed, James Bay lowland, Canada, J. Geophys. Res., 112, G01018, doi:10.1029/2006JG000216, 2007.

Petrescu, A. M. R., van Beek, L. P. H., van Huissteden, J., Prigent, C., Sachs, T., Corradi, C. A. R., Parmentier, F. J. W., and Dolman, A. J.: Modeling regional to global CH$_4$ emissions of boreal and arctic wetlands, Global Biogeochem. Cycles, 24, GB4009, doi:10.1029/2009GB003610, 2010.

25   Pickett-Heaps, C. A., Jacob, D. J., Wecht, K. J., Kort, E. A., Wofsy, S. C., Diskin, G. S., Worthy, D. E. J., Kaplan, J. O., Bey, I. and Drevet, J.: Magnitude and seasonality of wetland methane emissions from the Hudson Bay Lowlands (Canada), Atmos. Chem. Phys., 11, 3773–3779, doi:10.5194/acp-11-3773-2011, 2011.

Quay, P., Stutsman, J., Wilbur, D., Snover, A., Dlugokencky, E. J., Brown, T., The isotopic composition of atmospheric methane, Global Biogeochem. Cycles, 13(2), 445–461, doi:10.1029/1998GB900006, 1999.

30   Reshetnikov, A. I., Paramonova, N. N. and Shashkov, A. A.: An evaluation of historical methane emissions from the Soviet gas industry, J. Geophys. Res., 105(D3), 3517–3529, doi:10.1029/1999JD900761, 2000.

Rigby, M., Manning, A. J., and Prinn, R. G.: The value of high-frequency, high-precision methane isotopologue measurements for source and sink estimation, J. Geophys. Res., 117, D12312, doi:10.1029/2011JD017384, 2012.

Atmospheric
Chemistry
and Physics
Discussions

Open Access

EGU

Saueressig, G., Crowley, J. N., Bergamaschi, P., Brühl, C., Brenninkmeijer, C. A. M. and Fischer, H.: Carbon 13 and D kinetic isotope effects in the reactions of CH4 with O(1 D) and OH: New laboratory measurements and their implications for the isotopic composition of stratospheric methane, J. Geophys. Res., 106(D19), 23127–23138, doi:10.1029/2000JD000120, 2001.

5 Schaefer, H., Mikaloff Fletcher, S. E., Veidt, C., Lassey, K. R., Brailsford, G. W., Bromley, T. M., Dlugokencky, E. J., Englund Michel, S., Miller, J. B., Levin, I., Lowe, D. C., Martin, R. J., Vaughn, B. H., White, J. W. C.: A 21st-century shift from fossil-fuel to biogenic methane emissions indicated by $^{13}CH_4$, Science, 352, 80-84, doi: 10.1126/science.aad2705, 2016.

Shakhova, N., Semiletov, I., Salyuk, A., Yusupov, V., Kosmach, D., Gustafsson, Ö., Extensive methane venting to the
10 atmosphere from sediments of the East Siberian Arctic Shelf, Science, 327, 1246-1250, doi:10.1126/science.1182221, 2010.

Shakhova, N., Semiletov, I., Leifer, I., Sergienko, V., Salyuk, A., Kosmach, D., Chernykh, D., Stubbs, C., Nicolsky, D., Tumskoy, V. and Gustafsson, Ö.: Ebullition and storm-induced methane release from the East Siberian Arctic Shelf, Nature Geoscience, 7, 64–70, doi:10.1038/ngeo2007, 2014.

Song, C., Xu, X., Sun, X., Tian, H., Sun, L., Miao, Y., Wang, X. and Guo, Y.: Large methane emission upon spring thaw
15 from natural wetlands in the northern permafrost region, Environ. Res. Lett. 7 034009, doi:10.1088/1748-9326/7/3/034009, 2012.

Spivakovsky, C. M., et al.: Three-dimensional climatological distribution of tropospheric OH: Update and evaluation, J. Geophys. Res., 105(D7), 8931–8980, doi:10.1029/1999JD901006, 2000.

Sriskantharajah, S., Fisher, R. E., Lowry, D., Aalto, T., Hatakka, J., Aurela, M., Laurila, T., Lohila, A., Kuitunen, E. and
20 Nisbet, E. G., Tellus B, 64, 18818, http://dx.doi.org/10.3402/tellusb.v64i0.18818, 2012.

Sundqvist, E., Crill, P., Mölder, M., Vestin, P., and Lindroth, A.: Atmospheric methane removal by boreal plants, Geophys. Res. Lett., 39, L21806, doi:10.1029/2012GL053592, 2012.

Tan, Z. and Zhuang, Q.: Arctic lakes are continuous methane sources to the atmosphere under global warming, Environ. Res. Lett., 10, 054016, doi:10.1088/1748-9326/10/5/054016, 2015.

25 Tyler, S. C., Rice, A. L. and Ajie, H. O.: Stable isotope ratios in atmospheric CH4: Implications for seasonal sources and sinks, J. Geophys. Res., 112, D03303, doi:10.1029/2006JD007231, 2007.

Umezawa, T., Machida, T., Ishijima, K., Matsueda, H., Sawa, Y., Patra, P. K., Aoki, S. and Nakazawa, T.: Carbon and hydrogen isotopic ratios of atmospheric methane in the upper troposphere over the Western Pacific, Atmos. Chem. Phys., 12, 8095-8113, doi:10.5194/acp-12-8095-2012, 2012.

30 Van der Werf, G. R., Randerson, J. T., Giglio, L., Collatz, G. J., Kasibhatla, P. S., and Arellano, Jr., A. F.: Interannual variability in global biomass burning emissions from 1997 to 2004, Atmos. Chem. Phys., 6, 3423–3441, 2006.

Vaular, E. N., Barth, T., and Haflidason, H., The geochemical characteristics of the hydrate-bound gases from the Nyegga pockmark field, Norwegian Sea, Org. Geochem., 41(5), 437-444, doi:10.1016/j.orggeochem.2010.02.005, 2010.

Wang, J. S., Logan, J. A., McElroy, M. B., Duncan, B. N., Megretskaia, I. A., and R. M. Yantosca, R. M.: A 3-D model analysis of the slowdown and interannual variability in the methane growth rate from 1988 to 1997, Global Biogeochem. Cycles, 18, GB3011, doi:10.1029/2003GB002180, 2004.

Warwick, N. J., Pyle, J. A., Carver, G. D., Yang, X., Savage, N. H., O'Connor, F. M., and Cox, R. A.: Global modeling of biogenic bromocarbons, J. Geophys. Res., 111, D24305, doi:10.1029/2006JD007264, 2006.

Warwick, N. J., Archibald, A. T., Ashworth, K., Dorsey, J., Edwards, P. M., Heard, D. E., Langford, B., Lee, J., Misztal, P. K., Whalley, L. K., and Pyle, J. A.: A global model study of the impact of land-use change in Borneo on atmospheric composition, Atmos. Chem. Phys., 13, 9183-9194, doi:10.5194/acp-13-9183-2013, 2013.

White, J.W.C. and Vaughn, B. H.: University of Colorado, Institute of Arctic and Alpine Research (INSTAAR), Stable Isotopic Composition of Atmospheric Methane (13C) from the NOAA ESRL Carbon Cycle Cooperative Global Air Sampling Network, 1998-2014, Version: 2015-08-03, path: ftp://aftp.cmdl.noaa.gov/data/trace_gases/ch4c13/flask/, 2015.

White, J. W. C., Vaughn, B. H., and Michel, S. E.: University of Colorado, Institute of Arctic and Alpine Research (INSTAAR), Stable Isotopic Composition of Atmospheric Methane (D/H) from the NOAA ESRL Carbon Cycle Cooperative Global Air Sampling Network, 2005-2009, Version: 2016-04-26, Path: ftp://aftp.cmdl.noaa.gov/data/trace_gases/ch4h2/flask/, 2016.

Worthy, D. E. J., Chan, E., Ishizawa, M., Chan, D., Poss, C., Dlugokencky, E. J., Maksyutov, S., and Levin, I.: Decreasing anthropogenic methane emissions in Europe and Siberia inferred from continuous carbon dioxide and methane observations at Alert, Canada, J. Geophys. Res., 114, D10301, doi:10.1029/2008JD011239, 2009.

Yamada, K., Yoshidaa, N., Nakagawa, F., Inoue, G., Source evaluation of atmospheric methane over western Siberia using double stable isotopic signatures, Organic Geochemistry, 36, 717–726, doi:10.1016/j.orggeochem.2005.01.016, 2005.

Zona, D., Gioli, B., Commane, R., Lindaas, J., Wofsy, S. C., Miller, C. E., Dinardo, S. J., Dengel, S., Sweeney, C., Karion, A., Chang, R. Y.-W., Henderson, J. M., Murphy, P. C., Goodrich, J. P., Moreaux, V., Liljedahl, A., Watts, J. D., Kimball, J. S., Lipson, D. A., and Oechel, W. C., Cold season emissions dominate the Arctic tundra methane budget, Proc. Natl. Acad. Sci., 113, 40-45, doi: 10.1073/pnas.1516017113, 2016.
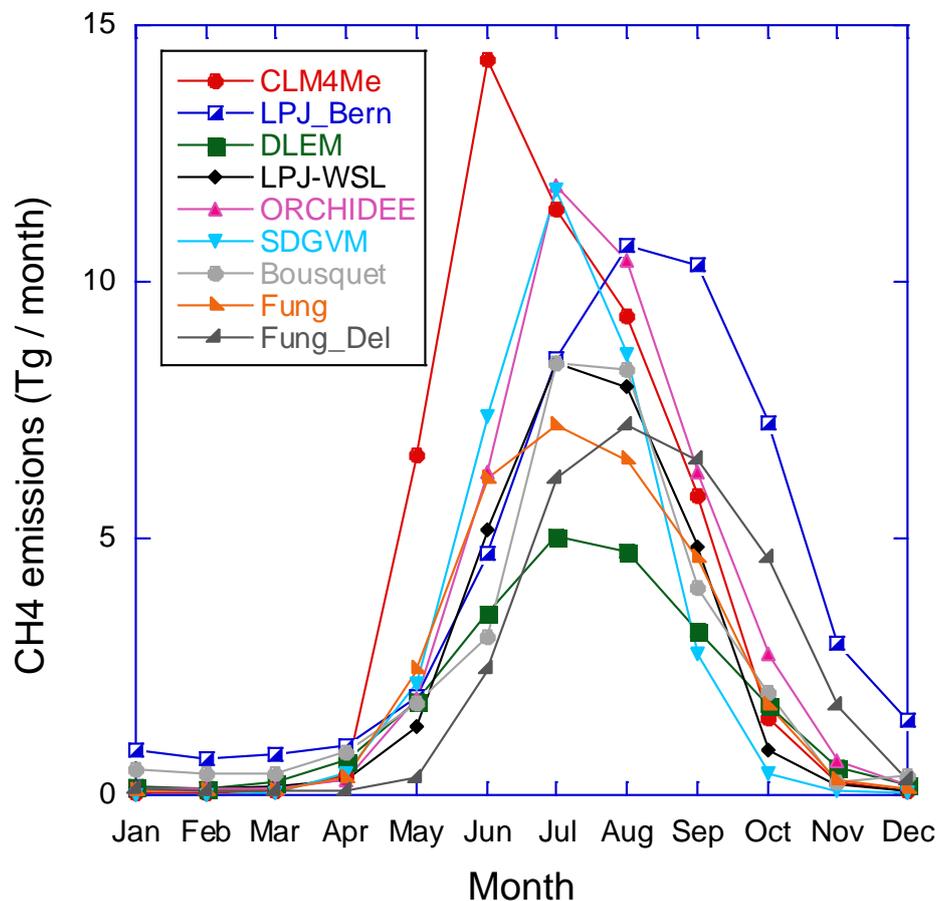
Figure 1: A comparison of seasonal cycles in northern wetland emissions (>50° N) from Fung et al. (1991) (Fung), Fung et al. (1991) with a seasonal cycle delayed by one month (Fung_Del), mean annual emission data for 1993-2004 from wetland process models obtained as part of the recent WETCHIMP model comparison (CLM4Me, LPJ_Bern, DLEM, WSL, ORCHIDEE, SDGVM; Melton et al., 2013) and mean annual emission data for 1993-2004 from the methane model inversion study of Bousquet et al., (2011).
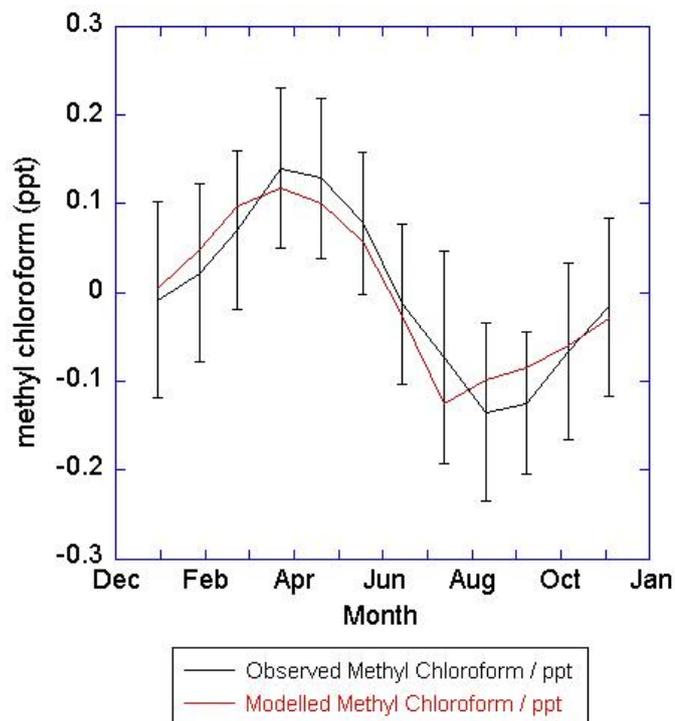
Atmospheric
Chemistry
and Physics
Discussions

Open Access

EGU

Figure 2: A comparison of observed and modelled seasonal cycles for methyl chloroform at Barrow, Alaska (157ºW, 71ºN). NOAA-ESRL observations are shown in black and are for the year 2011; error bars show +/- 1 s.d.. Model data uses 2011 meteorology and is shown in red. Linear trends and annual mean mixing ratios have been removed from both the observational and modelled data.
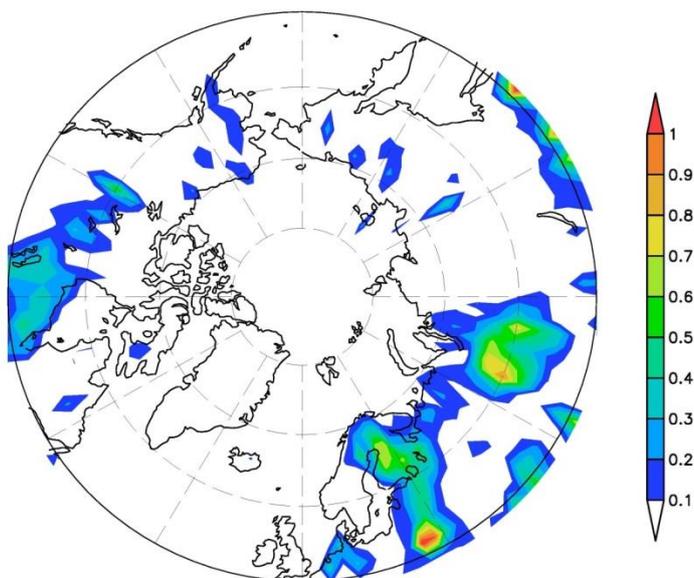
Figure 3: The geographical distribution of wetland emissions (mg/m^2/hr) above 50º N used in the model simulations. Emissions are based on Fung et al., 1991.

5

10

Atmospheric
Chemistry
and Physics
Discussions
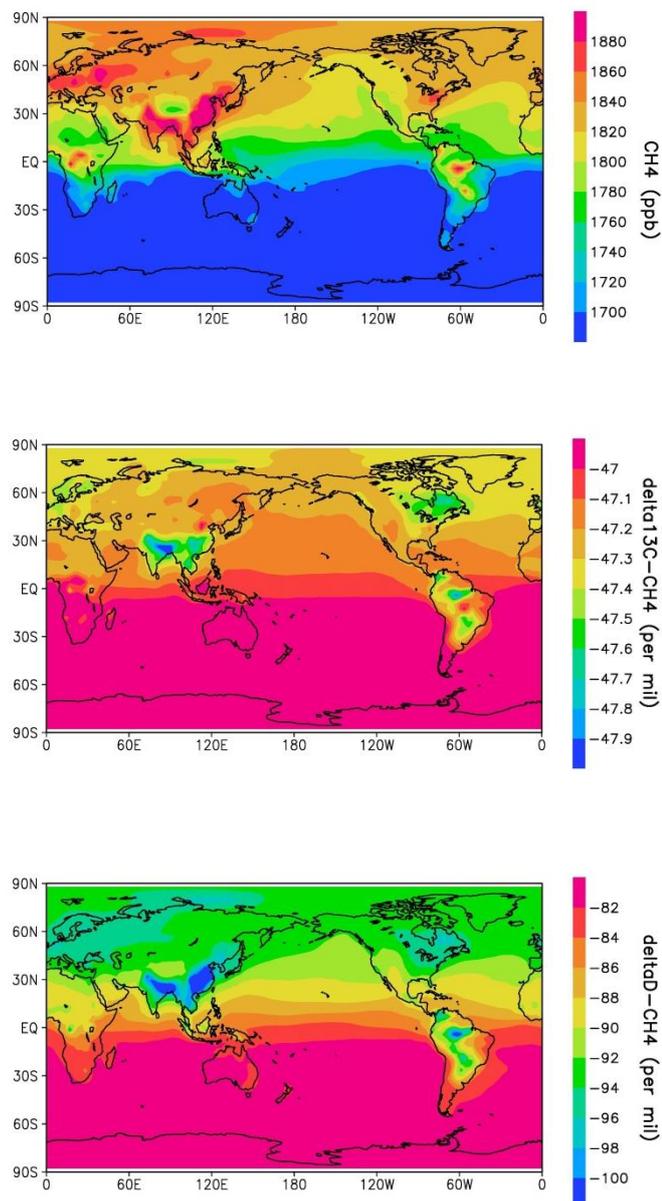
Figure 4: Modelled global annual mean surface distributions of CH₄, δ¹³C-CH₄ and δD-CH₄ for the p-TOMCAT BASE scenario.

5

10

Atmospheric
Chemistry
and Physics
Discussions

Open Access
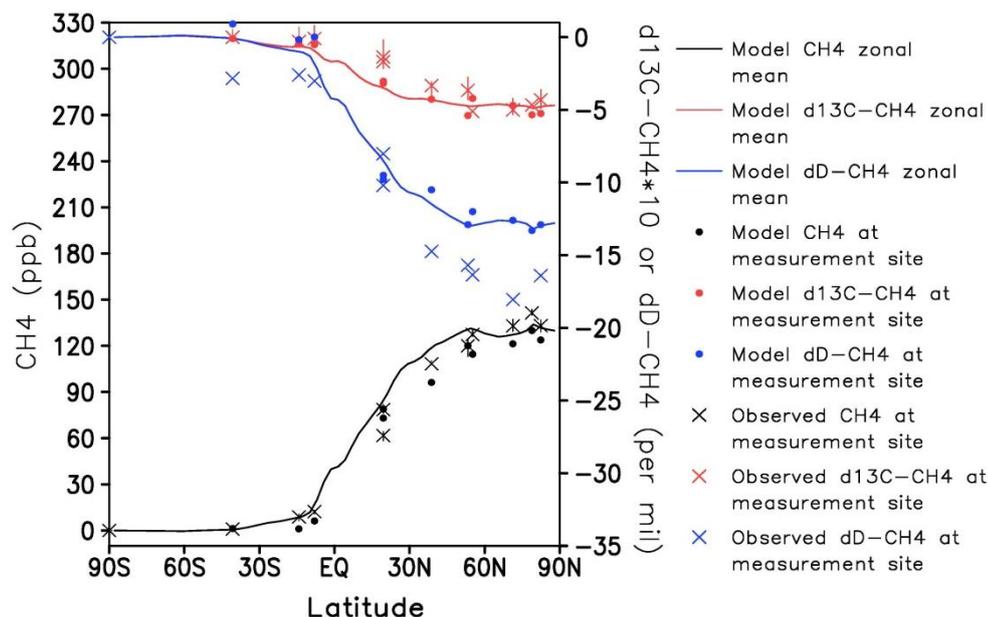
5 **Figure 5: The difference between surface annual mean CH$_4$, δ^{13}C-CH$_4$ and δD-CH$_4$ and South Pole annual mean values for CH$_4$, δ^{13}C-CH$_4$ and δD-CH$_4$. Results from the p-TOMCAT BASE scenario (including sampling the model at station locations) are compared to NOAA-ESRL and CU-INSTAAR observations. Where there are sufficient data available in the 2005 to 2009 period, the range in annual mean station-South Pole observed differences is represented by a vertical bar. CH$_4$ mixing ratios are shown in black, δ^{13}C-CH$_4$ in red and δD-CH$_4$ in blue. Variations in δ^{13}C-CH$_4$ have been multiplied by a factor of 10.**

10

Figure 6: A comparison of modelled seasonal cycles of CH$_4$, δ^{13}C-CH$_4$ and δD-CH$_4$ from the p-TOMCAT BASE scenario and NOAA-ESRL and CU-INSTAAR observations. Annual means have been subtracted from both the model and measurement data.
5 **Variations in δ^{13}C-CH$_4$ have been multiplied by a factor of 10. Where there are sufficient data available in the 2005 to 2009 period, the range of observed monthly mean values relative to the annual mean is represented by a vertical bar.**
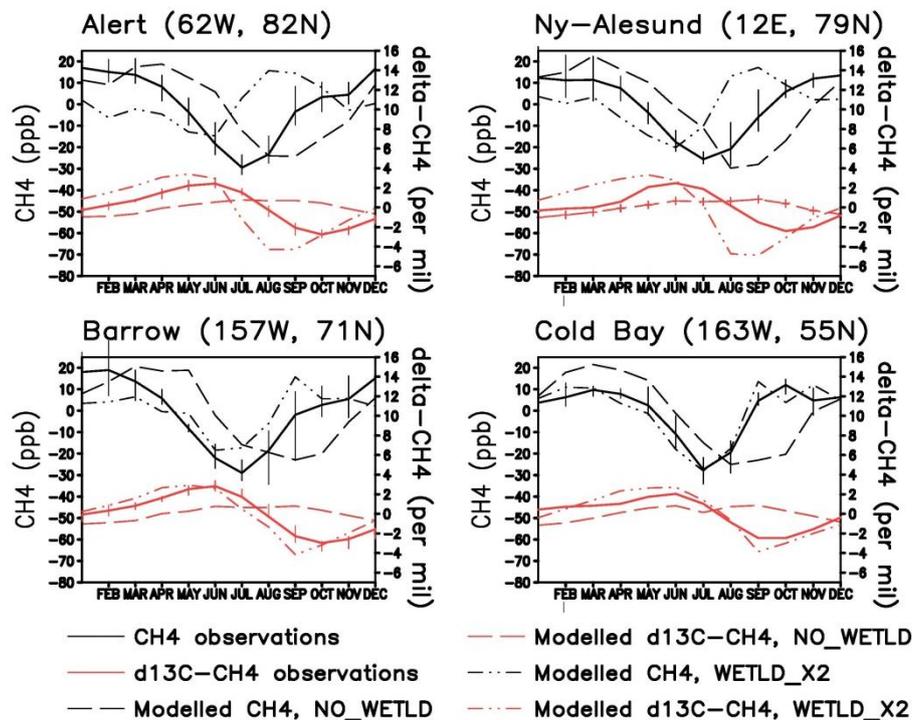
Figure 7: Modelled seasonal cycles of CH_4 and $\delta^{13}C$-CH_4 compared to NOAA-ESRL and CU-INSTAAR observations. Annual means have been subtracted from both the model and measurement data. Black represents CH_4 mole fractions and red represents $\delta^{13}C$-CH_4. Where there are sufficient data available in the 2005 to 2009 period, the range of observed monthly mean values relative to the annual mean is represented by a vertical bar. Dashed lines represent model results from the NO_WETLD scenario (where wetland emissions >50° N have been removed relative to BASE). Dot-dot-dash lines represent model results from the WETLD_X2 scenario (where wetland emissions >50° N have been increased by 50 % relative to BASE). Variations in $\delta^{13}C$-CH_4 have been multiplied by a factor of 10.

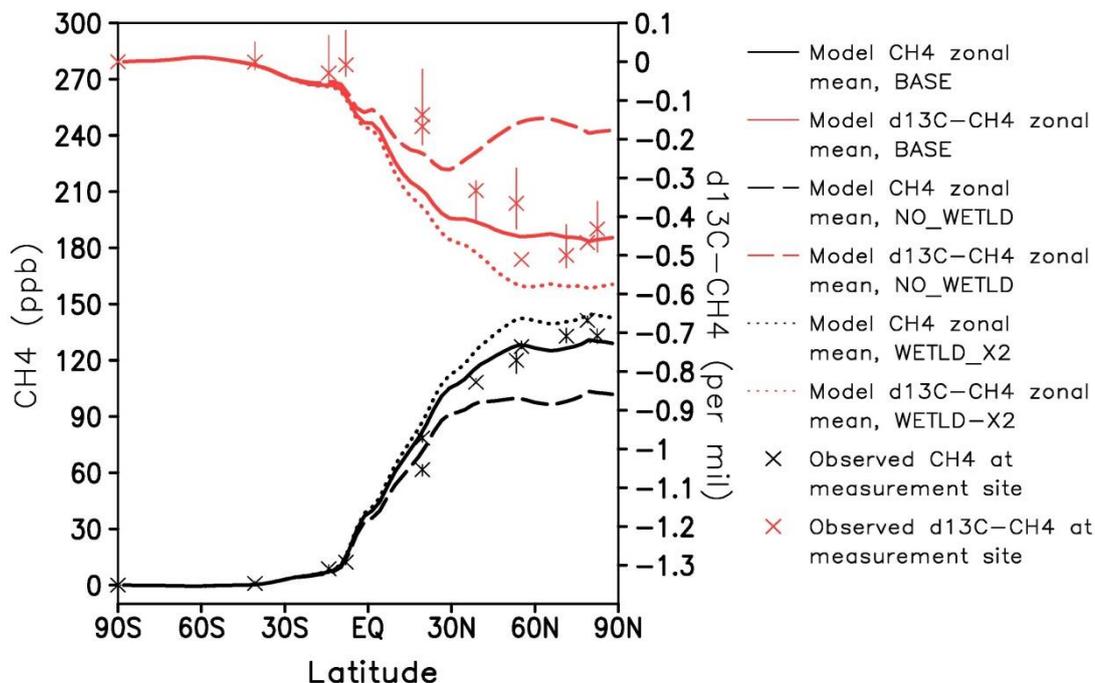**Figure 8: The difference between surface annual mean CH$_4$ and δ^{13}C-CH$_4$ and South Pole annual mean values. Model results are compared to NOAA-ESRL and CU-INSTAAR observations. Black represents CH$_4$ mixing ratios and red, δ^{13}C-CH$_4$ fractionations. Where there are sufficient data available in the 2005 to 2009 period, the range in annual mean station-South Pole observed differences is represented a vertical bar. Solid lines represent model results from the BASE scenario. Dashed lines represent model results from the NO_WET scenario (where wetland emissions >50° N have been removed relative to BASE). Dotted lines represent model results from the WETLD_X2 scenario (where wetland emissions >50° N have been increased by 50 % relative to BASE).**
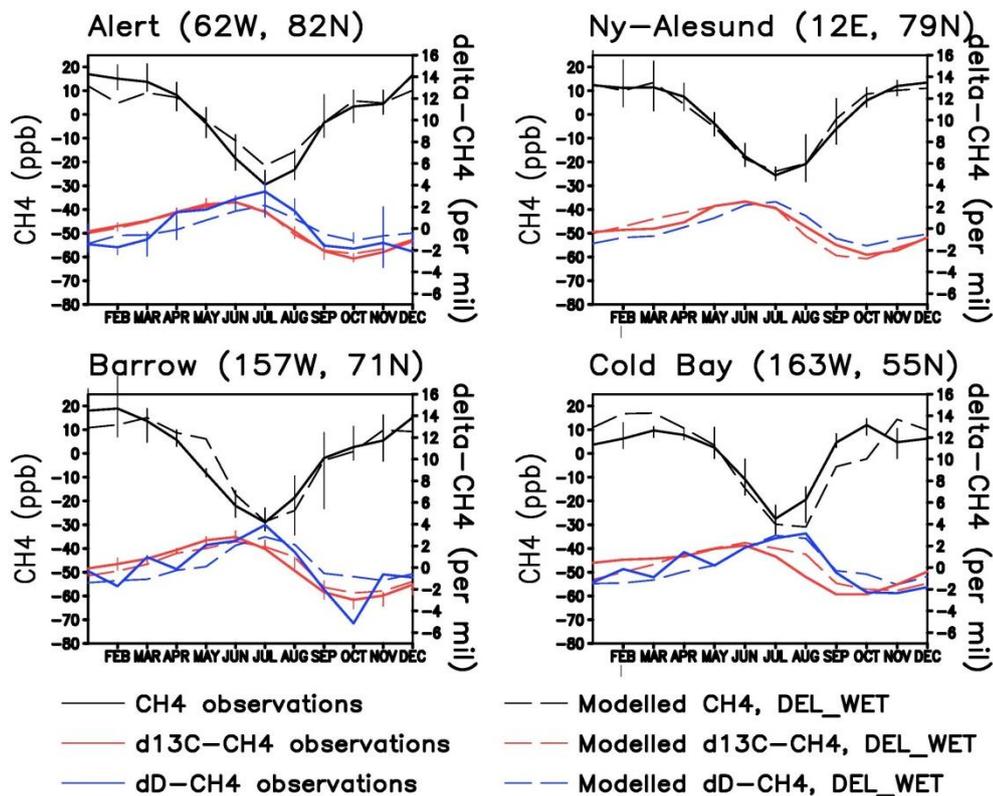
Atmospheric
Chemistry
and Physics
Discussions

Figure 9: As Figure 3, except showing model results from the DEL_WET scenario (where the seasonal cycle of wetland methane emissions from >50° N has been delayed by one month relative to BASE). Variations in δ^{13}C-CH$_4$ have been multiplied by a factor of 10.
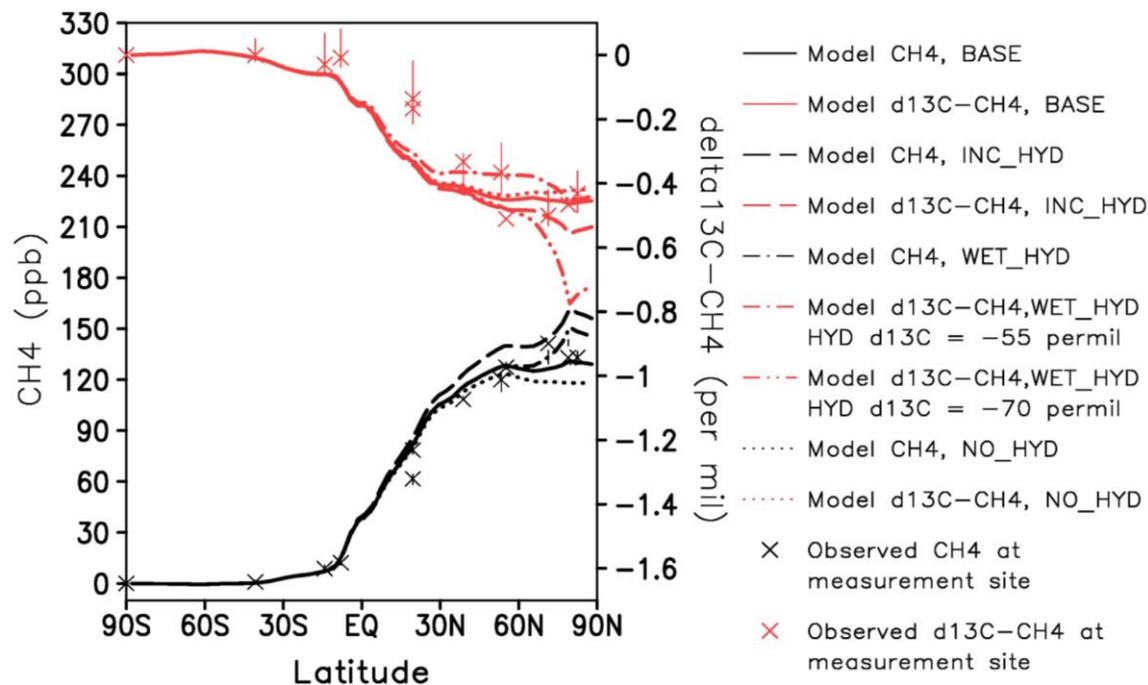
5

Figure 10: The difference between surface annual mean modelled latitudinal gradients in CH$_4$ and δ^{13}C-CH$_4$ and South Pole annual mean values. Model results are compared to NOAA-ESRL and CU-INSTAAR observations. Black represents CH$_4$ mixing ratios and red, δ^{13}C-CH$_4$ fractionations. Where there are sufficient data available in the 2005 to 2009 period, the range in annual mean station-South Pole observed differences is represented a vertical bar. Solid lines represent model results from the BASE emission scenario. Dashed lines represent model results from the INC_HYD scenario (where hydrate emissions have been increased by 12 Tg yr^{-1} to 17 Tg yr^{-1} relative to BASE). Dotted lines represent model results from the NO_HYD scenario (where emissions from methane hydrates are removed relative to BASE). Dot-dash lines show model results from the WET_HYD scenario (where hydrate emissions are increased by 12 Tg yr^{-1} to 17 Tg yr^{-1} and wetland emissions > 50° N are reduced by 12 Tg yr^{-1} relative to BASE). Dot-dot-dash lines represent emission magnitudes as for the WET_HYD scenario, but with an isotopic fractionation for hydrate emissions of -70‰.